Analytic Solution for the Birefringence Produced by Thermal Stress in Polarization-Maintaining Optical Fibers

MALCOLM P. VARNHAM, DAVID N. PAYNE, ARTHUR J. BARLOW, AND ROBIN D. BIRCH

Abstract—**Polarization-maintaining optical fibers are usually made by inducing a large anisotropic thermal stress in the core so that it appears highly birefringent. A simple analytic solution has been found for the birefringence in terms of the cross-sectional distribution of the high-expansion material used to create the thermal stress. The analysis is able to predict optimal structures which efficiently utilize the available stress and thus maximize the birefringence. It is shown that the optimum structure has a cross-sectional geometry resembling a bow-tie. Design rules are given whereby the dimensions may be chosen and these are verified in a simple experiment.**

I. Introduction

COHERENT transmission systems using the optical heterodyne principle require a stable polarization state for both the local oscillator and incoming signal waves [1]. Interferometric fiber sensors similarly require colinearity between the polarization states emerging from the sensor and reference arms [2]. Unfortunately, bends, twists, and side pressure [3] introduce small amounts of birefringence into the fiber which vary with time, causing the output polarization state to vary accordingly. Thus for a conventional monomode fiber the output polarization state is indeterminate and this causes considerable difficulties in a number of applications.

A fiber may be designed to be relatively immune to environmental effects by deliberately increasing its intrinsic birefringence $\Delta\beta$ to a level far greater than that produced by external perturbations. External variations are then swamped and highly birefringent fibers can transmit linearly polarized light aligned with one of the principal axes [4] over long distances. Although core ellipticity alone can contribute a waveguide-related birefringence [5], fibers are normally made birefringent by introducing a large thermal-stress anisotropy in the core. This can be achieved by employing materials having a large expansion coefficient embedded asymmetrically within the fiber cross section. For example, a common approach is to employ an elliptical stress-producing region of highly doped silica material within a circular silica substrate. Such fibers have exhibited very high birefringence and good polarization-holding ability [6].

Photo-elastically induced birefringence has been analyzed by several authors. The first analysis [7] was based on a slab model with an infinite substrate. More recently, fibers with an elliptical core surrounded by 1) an infinite cladding [8] and 2) a finite cladding, [9] have been analyzed in elliptical coordinates. So called side-pit, elliptical core, elliptical jacket, and azimuthally inhomogeneous optical fibers have also been analyzed using finite elements [10]-[14]. The limitation of all these analyses is that they are either specific to a given geometry, or computationally cumbersome to the extent that optimization of the birefringence and performance of new structures is difficult to predict.

We present here a new and remarkably simple analysis [15] of thermal-stress birefringence in optical fibers. The approach has the advantage that it provides an intuitive formulation, leading directly and obviously to the optimum structure which maximizes the birefringence for a given expansion coefficient mismatch. It is shown that this optimum structure resembles a bow-tie in cross-sectional shape. Furthermore, some results are presented on bow-tie fibers which have been fabricated by a new and novel technique, reported elsewhere [15], [16].

Elliptical core, elliptical jacket, and circular side-pit fibers are also analyzed, and the results, though very simply derived, are shown to agree with specific cases previously reported [9]-[14]. In addition, it is confirmed that the dimensions of the substrate within which the stress-producing region is embedded has a considerable effect on the birefringence, a finding which was reported in [13]. This effect is verified in an experiment where the birefringence of a fiber was measured as the substrate material was successively removed.

II. Derivation of the Formula for Thermal-Stress Birefringence

When a composite glass fiber is drawn at high temperature from a viscous melt or preform, thermal stresses can develop once the fiber cools through the temperature at which the glass sets. Further cooling results in an increase in stress owing to the different thermal contraction of the materials within the fiber. Thermal stresses in fibers of circular cross-sectional coordinates (r, Θ) (Fig. 1(a)) containing asymmetrically disposed regions of a different thermal-expansion coefficient (Fig. 1(b)) may be calculated by solving the differential equation for plane strain [17]. The solution is accomplished in

Manuscript received January 7, 1983. This work was supported by Research Fellowships from Pirelli General Cable Company (DNP), the UK Science and Engineering Research Council (RDB), and British Aerospace (AJB). A Research Studentship (MPV) was also provided by British Aerospace.

M. P. Varnham, D. N. Payne, and R. D. Birch are with the Department of Electronics, University of Southampton, Southampton, England.

A. J. Barlow is now with the Department of Electronics, University of Southampton, Southampton, England. He is on leave from British Aerospace plc., Stevenage, Herts, England.

0733-8724/83/0600-0332$01.00 © 1983 IEEE

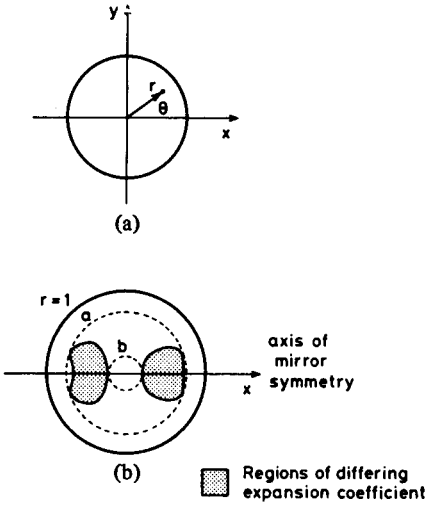

Fig. 1. (a) Coordinate system. (b) Cross section of fiber containing mirror-symmetric regions having differing expansion coefficients.

three parts, as follows.

1) The particular integral is sought via the thermoelastic displacement-potential function $\psi(r, \Theta)$, which is defined by the polar displacements $u = \partial\psi/\partial r$ and $v = (1/r)\,\partial\psi/\partial\Theta$. The thermal stresses and strains can be found from u and v, for example, the radial strain ϵ_r is given by $\epsilon_r = \delta u/\delta r$.

2) The complementary function is found from the general stress function $\phi(r, \Theta)$ for cylindrical bodies by assigning values to arbitrary constants which satisfy the boundary conditions. The stress function $\phi(r, \Theta)$ is defined by the relations $\sigma_r = (1/r)\,\partial\phi/\partial r$ and $\sigma_\Theta = \partial^2\phi/\partial r^2$, where σ_r and σ_Θ are the radial and hoop stresses, respectively.

3) The total solution is the sum of the particular integral and complementary function.

Once the stresses have been found, the normalized birefringence $B = (\lambda/2\pi)\,\delta\beta = -C(\sigma_x - \sigma_y)$ can be evaluated, where C is the stress-optic coefficient and $\sigma_x - \sigma_y$ is the stress difference in the core. For any fiber having one axis of mirror symmetry, a very simple equation results relating B to the expansion-coefficient profile.

A. Calculation of Thermal Stresses in Fibers

Following the method outlined by Timoshenko [17], the thermal stresses in a body with circular cross-section can be found from the thermoelastic displacement potential $\psi(r, \Theta)$ which satisfies the differential equation for plane strain

$$\nabla^2\psi(r,\Theta) = \frac{(1+\nu)}{(1-\nu)}\,\alpha(r,\Theta)\,T. \tag{1}$$

Here $\alpha(r,\Theta)$ is the thermal-expansion coefficient of the material located at position (r, Θ) in the fiber and ν is the Poisson's ratio, assumed to be the same for each component glass. T is the difference between ambient temperature T_0 and the temperature at which the glass sets, i.e., begins to behave elastically (the fictive temperature).

In practice, T depends on glass composition and is typically several hundred °C higher in the substrate than in the core. Thus the substrate sets before the core. Further cooling results only in hydrostatic stresses within the fluid core, until it in turn sets at temperature T_c and is then able to support anisotropic stresses. Since we are concerned here exclusively with the calculation of core anisotropic stress, the appropriate value of T is given by the setting point of the core, i.e.,

$$T = T_0 - T_c \tag{2}$$

where T_c is the core fictive temperature. Note, however, that if on cooling some regions of the fiber remain fluid after the core has set, it is strictly necessary to take into account the relatively large change in expansion coefficient which occurs as they pass through their respective setting temperatures. For simplicity, we shall ignore these induced stresses and assume that all constituent glasses set at or above the setting point of the core.

If $\alpha(r, \Theta)$ has mirror symmetry about the x-axis (see Fig. 1(b)), it can be expressed in Fourier series form

$$\alpha(r,\Theta) = \alpha_0(r) + \sum_{m=1}^{\infty} \alpha_m(r)\cos m\Theta \tag{3}$$

where $\alpha_0(r)$ is the average value of the expansion coefficient found at radius r and $\alpha_m(r)$ is the mth harmonic of $\alpha(r, \Theta)$ as a function of radius, given by

$$\alpha_m(r) = \frac{1}{\pi}\int_0^{2\pi} \alpha(r,\Theta)\cos m\Theta\, d\Theta. \tag{4}$$

Substituting (3) into (1) leads to the Fourier series expansion of the thermoelastic displacement potential $\psi(r,\Theta)$

$$\psi(r,\Theta) = \psi_0(r) + \sum_{m=1}^{\infty} \psi_m(r)\cos m\Theta \tag{5}$$

where $\psi_m(r)$ is given by the solutions of the differential equation

$$\frac{d^2\psi_m(r)}{dr^2} + \frac{1}{r}\frac{d\psi_m(r)}{dr} - \frac{m^2}{r^2}\psi_m(r) = \frac{(1+\nu)}{(1-\nu)}\alpha_m(r)\,T. \tag{6}$$

The solution of (6) is the sum of the particular integral and complementary function.

In the fiber, normalized radius $r = 1$, we now define an annular area $a > r > b$ which bounds the asymmetrically disposed regions having different expansion coefficients (see Fig. 1(b)). In regions $r > a$ and $r < b$ the harmonic content of $\alpha(r)$ is zero ($\alpha_m(r) = 0$ for $m \neq 0$), and the following particular integral is obtained [17]:

$$\psi_m(r) = -\frac{(1+\nu)}{(1-\nu)}\frac{r^m}{2m}\int_b^a \alpha_m(r)\,Tr^{1-m}\,dr = G_m r^m \tag{7}$$

for $r < b, m \neq 0$, and

$$\psi_m(r) = -\frac{(1+\nu)}{(1-\nu)}\frac{r^{-m}}{2m}\int_b^a \alpha_m(r)\,Tr^{1+m}\,dr = H_m r^{-m} \tag{8}$$

for $r > a, m \neq 0$.

As in all differential equations, the complementary function is given by a general equation containing arbitrary constants which are determined by the boundary conditions. Here, the

stresses arising from the complementary function can be described by a general stress function $\phi(r,\Theta)$ for $m \neq 0$ [17]

$$\phi(r,\Theta) = b_1 r^3 \cos\Theta + \sum_{m=2}^{\infty} (a_m r^m + b_m r^{m+2}) \cos m\Theta \tag{9}$$

where a_m and b_m are the arbitrary constants found by satisfying the boundary conditions at $r = 1$, namely that the normal and shear stresses are both zero [17].

B. Formula for the Thermal-Stress-Induced Birefringence

The ψ_0 component of (5) leads to symmetric thermal stresses which are independent of Θ [17] and, therefore, do not affect the birefringence. These stresses will not be considered further in this derivation, although they should not be forgotten since they contribute to the overall fiber and preform stress level. They may ultimately determine whether the preform shatters during fabrication and should, therefore, be minimized along with any other stresses which do not contribute to the birefringence.

To derive the birefringence produced by the anisotropic stress distribution we will sum the contributions from the particular integral and complementary function at the fiber center ($r = 0$). In principle the stresses in the whole fiber should be calculated and the birefringence found using coupled-mode theory [3], [9]. This approach is more rigorous since the optical field extends over core and cladding regions, in which the stresses vary slightly. The optical spot size depends on the fiber V-value and consequently so will the birefringence. However, in this section we will make the simplifying assumption that the field is confined at $r = 0$, and, therefore, is only affected by stresses at the fiber center. This assumption has also been used in the finite element analyses, and is known to give good results [9]-[14] if the core is circular and the field well confined (i.e., $V \sim 2.4$).

The radial strain ϵ_r which results from the particular integral (7) is given [17] from (3) and (7) by

$$\epsilon_r(r,\Theta) = \frac{\partial^2 \psi}{\partial r^2}(r,\Theta) = \sum_{m=2}^{\infty} m(m-1) G_m r^{m-2} \cos m\Theta. \tag{10}$$

Approximating the strains ϵ_x and ϵ_y in the core by $\epsilon_r(0,0)$ and $\epsilon_r(0, \pi/2)$, respectively, we obtain for the birefringence B_p resulting from the particular integral

$$B_p = -\frac{CE}{1+\nu}(\epsilon_x - \epsilon_y) = -\frac{4CE}{1+\nu} G_2 \tag{11}$$

where C and E are the stress-optic coefficient and Young's modulus, respectively. Note that focusing our attention on the birefringence alone has reduced the problem such that only the 2nd harmonic coefficient G_2 in G_m need be considered.

Similarly, the radial stress σ_r resulting from the complementary function (9) is given by [17]

$$\sigma_r(r,\Theta) = \frac{1}{r}\frac{\partial \phi}{\partial r} + \frac{1}{r^2}\frac{\partial^2 \phi}{\partial \Theta^2}$$

which, from (9) leads to

$$\sigma_r(r,\Theta) = 2b_1 r \cos\Theta + \sum_{m=2}^{\infty} \{(m - m^2) a_m r^{m-2} + (2 + m - m^2) b_m r^m\} \cos m\Theta. \tag{12}$$

Again, approximating σ_x and σ_y in the core by $\sigma_r(0,0)$ and $\sigma_r(0, \pi/2)$, respectively, we obtain for the birefringence B_c resulting from the complementary function

$$B_c = -C(\sigma_x - \sigma_y) = 4Ca_2. \tag{13}$$

Again, it is only the arbitrary constant a_2 associated with the second-haromonic stress component which is of importance.

The constant a_2 can be found from the boundary condition that the net radial stress $\sigma_r = 0$ at $r = 1$, which, by the uniqueness theorem of Fourier analysis, implies that $\sigma_r = 0$ for each stress harmonic. The second-harmonic stress contribution to σ_r from the complementary function is given by the term $m = 2$ in (12). Similarly, the second-harmonic stress contribution to σ_r from the particular integral in $r > a$ is found by substituting $\psi_2 = H_2 r^{-2} \cos 2\Theta$ into

$$\sigma_r = \frac{E}{(1-2\nu)(1+\nu)}\left[(1-\nu)\frac{\partial^2 \psi_2}{\partial r^2} + \nu\left\{\frac{1}{r}\frac{\partial \psi_2}{\partial r} + \frac{1}{r^2}\frac{\partial^2 \psi_2}{\partial \Theta^2}\right\}\right] \tag{14}$$

where H_2 is defined by (8). The net second-harmonic stress contribution to σ_r in $r > a$ is then given by the sum of the contributions from the complementary function and particular integral, which from the above is

$$\sigma_r = -2a_2 \cos 2\Theta + \frac{6EH_2}{1+\nu} r^{-4} \cos 2\Theta. \tag{15}$$

Inserting the boundary condition $\sigma_r = 0$ at $r = 1$ yields a_2 and, hence, from (13)

$$B_c = \frac{12CE}{(1+\nu)} H_2. \tag{16}$$

Thus we have the final result from (7), (8), (11), and (16) that the thermal-stress-induced modal birefringence $B = B_p + B_c$ in a circular fiber of normalized radius $r = 1$ is

$$B = (n_x - n_y) = \frac{CE}{(1-\nu)} \int_b^a \alpha_2(r)\, T(r^{-1} - 3r^3)\, dr \tag{17}$$

where $\alpha_2(r)$ is the second-harmonic component of $\alpha(r,\Theta)$ as a function of r, and is given by

$$\alpha_2(r) = \frac{1}{\pi} \int_0^{2\pi} \alpha(r,\Theta) \cos 2\Theta\, d\Theta. \tag{18}$$

It should be noted that these equations are only valid for circular fibers having mirror symmetry about the x-axis. The derivation could be extended to cover a more general case [17], but at the expense of the simplicity of (17) and (18). Moreover, this symmetry restriction is not a serious one, since the present analysis holds for most fibers of practical interest.

Note also that the stress difference $\sigma_x - \sigma_y$ can be shown to

be constant for $r < b$ and $m = 2$. Thus the stress-induced birefringence will also be constant within the region. This fact increases the validity of our assumption that the optical field is confined at $r = 0$, since in many fiber designs the optical power will be totally contained within $r < b$ and will, therefore, experience a uniform stress-field, even if the core is not exactly centrally located.

III. Physical Interpretation of the Analysis

A. Two Important Results

1) Consider a fiber with an arbitrary mirror-symmetric distribution of material with expansion coefficient $\alpha(r, \Theta)$, embedded within a fiber of circular cross section, such as that shown in Fig. 1(b). The intuitive nature of (17) can be readily seen by noting that to determine the birefringence we need only consider the azimuthal *second-harmonic content* $\alpha_2(r)$ (i.e., frequency 2Θ) of the expansion coefficient $\alpha(r, \Theta)$ within the annular region bounded by $a > r > b$. The second-harmonic content $\alpha_2(r)$ can be visualized from plots such as that in Fig. 3, which charts the expansion coefficient as a function of azimuth Θ around a circle of radius r. We are interested solely in the magnitude of the 2Θ frequency component of $\alpha(r, \Theta)$ (i.e., period π rad); consequently it is immediately clear that fibers with triangular, square, etc., high-expansion regions centered on-axis contribute no birefringence at all, since they possess no component of frequency 2Θ. Similarly, concentric circular regions can be ignored. These structures merely add to the general level of stress within the fiber or preform and should be avoided, since they increase the probability of the preform shattering.

As an example, let us take a fiber with an elliptical stress-producing region, as shown in Fig. 2(d). The value of $\alpha_2(r)$ is zero for $b > r > a$ and we, therefore, consider only the annular region $a > r > b$. In this region $\alpha_2(r)$ increases from zero around the circle defined by $r = b$, to a maximum at the radius where the ellipse intersects the straight line $y = x$, and then decreases to zero again. Consequently, a large proportion of the elliptical high-expansion jacket does not contribute to the birefringence (i.e., that contained within the circle $r < b$) and, furthermore, the section confined within the annular region $a > r > b$ has a poor second-harmonic content. This structure clearly utilizes the available high-expansion material inefficiently.

Since the preform can only support a given level of stress before shattering, stresses from "waste" harmonics (i.e., fourth, sixth, etc. which are present, for example, in the elliptical jacket fiber), and regions with circular symmetry, should be minimized to enable all the available stress to contribute to the birefringence.

2) The two terms r^{-1} and $-3r^3$ in (17) come from the particular integral and complementary function, respectively, and are of opposite sign. Consequently, they sum to zero at fiber radius $r_0 = (3)^{-1/4} \simeq 0.76$. This is an important result, since it indicates that any asymmetry present at a radius greater than r_0 *reduces* the birefringence. The asymmetrically disposed high-expansion material should, therefore, always be contained within a radius less than 0.76 of the fiber outer radius.

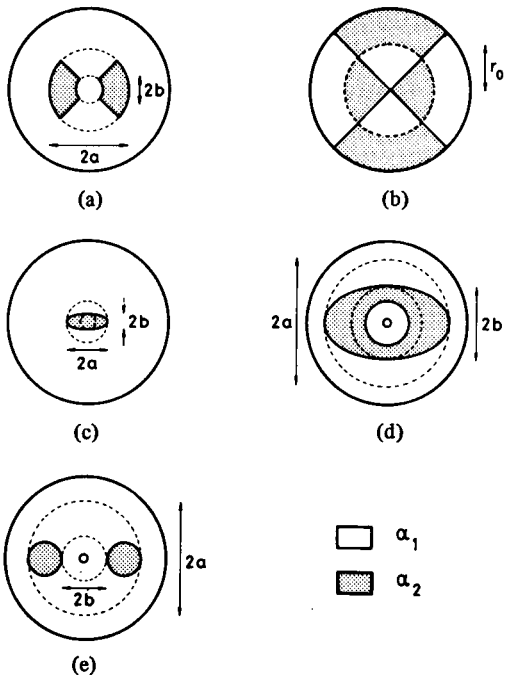

Fig. 2. Cross-sectional distribution of high-expansion material for various stress-producing structures reported in the literature.

B. The Optimum Structure for Maximum Birefringence

We define the optimum structure as that distribution of high-expansion coefficient material which will maximize the birefringence for a given maximum expansion-coefficient mismatch $\Delta\alpha = (\alpha_{MAX} - \alpha_{MIN})$. We chose this criterion since the maximum mixmatch is normally limited by material constraints, for example, the maximum dopant concentration which can be incorporated in the high-expansion regions is usually limited. From (17) we have seen that to optimize the birefringence it is only necessary to maximize $\alpha_2(r)$, the second-harmonic content of $\alpha(r, \Theta)$. It is well known that the waveform which has highest second-harmonic content for a given peak-to-peak value $\Delta\alpha$ is a square wave of frequency 2Θ with equal mark-space ratio, for which $\alpha_2(r) = 2(\Delta\alpha)/\pi$. The material distribution represented by such a waveform resembles a bow-tie with 90° sectors and is illustrated in Fig. 2(a). The outer radius a of the sectors must be less than 0.76 of the fiber radius, as noted earlier. However, some additional birefringence can be achieved by changing the sense of $\alpha(r, \Theta)$ at radius r_0 as illustrated in Fig. 2(b).

Recently we have reported a gas-phase-etching fabrication technique [15], [16] whereby "bow-tie" fibers can be readily manufactured. These fibers have exhibited polarization beat-lengths as short as 0.55 mm at a wavelength of 633 nm, a figure which at the time of writing is the shortest ever reported. The result is attributable to the adoption of the optimum structure developed here. Two other fibers [18], [19] with similar geometry made by different techniques have also been reported. Although not optimized for birefringence, these fibers have given good results, further indicating the advantage of adopting the optimum bow-tie configuration.

If the maximum value of $\alpha(r, \Theta)$ is not a constraint, it is possible to define another "optimum" structure as that which most efficiently uses the available stress to produce birefringence.

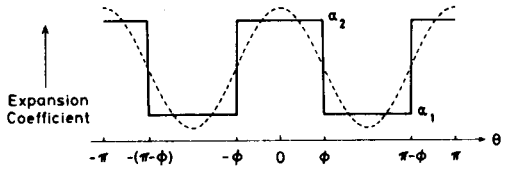

Fig. 3. Typical azimuthal variation of expansion coefficient at a constant radius r for the structures of Fig. 2.

A sinusoidal distribution of high-expansion material to give a $\cos 2\Theta$ dependence of $\alpha(r,\Theta)$ has $\alpha_2(r) = (\Delta\alpha)/2$ and no "wasted" harmonics to add to the general stress level in the fiber. These structures are the sinusoidal equivalents of the square-wave distributions shown in Fig. 2(a) and 2(b). For the same value of α_{MAX} the birefringence produced is 21-percent lower than for the bow-tie fibers, although greater stress efficiency and thus lower net stress levels may lessen the chance of the preform shattering.

IV. Analysis of Four Different Structures

In this section we quantitatively analyze birefringence in the bow-tie [15], [16], the elliptical core [8]-[10], the elliptical cladding [12], [13], and the circular side-pit [11] fiber geometries shown in Fig. 2. The results lead directly to suggested dimensions for the asymmetries.

A. Analysis

From Section III, we note that uniform circular regions of different α, such as cores and claddings, do not contribute to the birefringence and thus the analysis for the elliptical core (Fig. 2(c)) and elliptical jacket (Fig. 2(d)) fibers are identical (neglecting the usually small contribution due to waveguide birefringence produced by the elliptical core). Each structure is assumed to be composed of two materials with expansion coefficients α_1 and α_2 (Fig. 2) and have a normalized outer radius $r = 1$. In each case, an asymmetry exists in the annular region $a > r > b$ where, following a circle of constant r, $\alpha(r,\Theta)$ describes a square wave in Θ with maximum and minimum amplitudes of α_2 and α_1 respectively. Fig. 3 illustrates the value of $\alpha(r,\Theta)$ as a function of Θ for one value of r in a typical fiber, together with the second-harmonic ($\cos 2\Theta$) component which determines the birefringence. The latter has an amplitude $2/\pi$. $\Delta\alpha \sin 2\theta$, where $\Delta\alpha = \alpha_2 - \alpha_1$ and ϕ is the angle at which the boundary of the stress-producing region intersects the circle at radius r. For the bow-tie fiber the $\cos 2\Theta$ amplitude is constant in $a > r > b$, whereas it increases from zero to a maximum and back to zero with increasing r for the other fibers. From (17) and (18), the modal birefringence is simply

$$B = \frac{CE}{1-\nu}\frac{2}{\pi}(\Delta\alpha)\,T\int_b^a \sin 2\phi(r^{-1} - 3r^3)\,dr \tag{19}$$

where ϕ is constant for the bow-tie fiber, and for fibers with elliptical stress-producing regions (Fig. 2(c) and 2(d)) is given by

$$\cos^2\phi = \frac{a^2(r^2 - b^2)}{(a^2 - b^2)r^2}, \quad a > r > b. \tag{20}$$

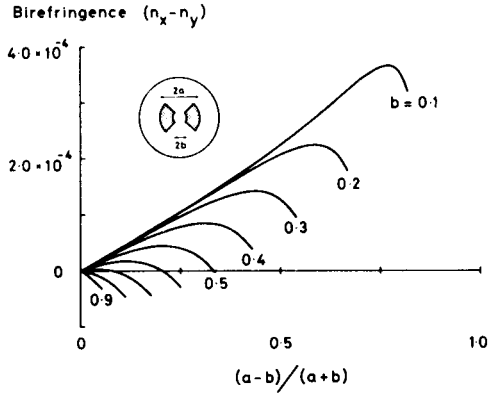

Fig. 4. Variation of modal birefringence with cross-sectional geometry in a bow-tie fiber plotted for various values of b, the inner radius of the stress-producing sectors.

For fibers with asymmetric circular stress-producing regions (Fig. 2(e)):

$$\cos\phi = \frac{r^2 + ab}{r(a+b)}, \quad a > r > b. \tag{21}$$

In the following, (19) has been integrated to give curves of B versus $(a-b)/(a+b)$ for constant values of b. In each case, we have taken $C = -3.36 \times 10^{-5}$ mm^2/kg, $E = 7830$ kg/mm^2, $\nu = 0.186$, and $(\Delta\alpha)\,T = 10^{-3}$ to enable direct comparison between the structures.

B. Bow-Tie Fibers

For this structure, (19) can be integrated directly to give

$$B = \frac{2}{\pi}\frac{EC}{1-\nu}(\Delta\alpha)\,T\sin 2\phi\left\{\ln\left(\frac{a}{b}\right) - 0.75\,(a^4 - b^4)\right\}. \tag{21}$$

The value of B is plotted in Fig. 4 for $2\phi = 90°$ (the optimum sector angle). Each curve represents a constant value of b as a is varied. From the figure, we see that the largest birefringence occurs for small b, indicating that the bow-tie sectors should be as close to the core as possible. The curves reach a maximum birefringence at a value of $(a-b)/(a+b)$ corresponding to $a = r_0 = 0.76$, as noted earlier. When $a > r_0$ the birefringence decreases and can become negative when the sectors are positioned totally outside the radius r_0 (i.e., $a > b > r_0$). In this case, the fast and slow axes of the birefringence are interchanged and the effect can be used to advantage in the structure proposed in Fig. 2(b).

It is interesting to note that if $2\phi = 30°$, i.e., the bow tie is thinner, the birefringence only halves. This is because it is the second-harmonic component and not the degree of asymmetry that is important. Thus precise control of the angular shape of the sectors is not critical.

Note also that as $b \to 0$ the fiber assumes the geometry analyzed by Chu [14], called the "azimuthally inhomogeneous" fiber. We see from (21) that for this structure the stress at $r = 0$ is infinite and that, therefore, the structure cannot be made without cracking. However, if b is made small, but not zero, it is clear that very large stresses can result. In this case, the

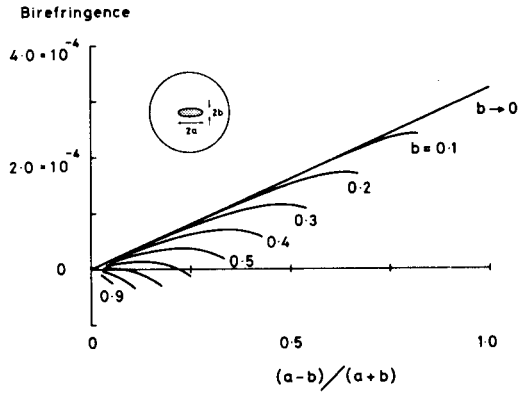

Fig. 5. Variation of modal birefringence with ellipticity in an elliptical core or jacket fiber plotted for various values of b, the ellipse minor axis.

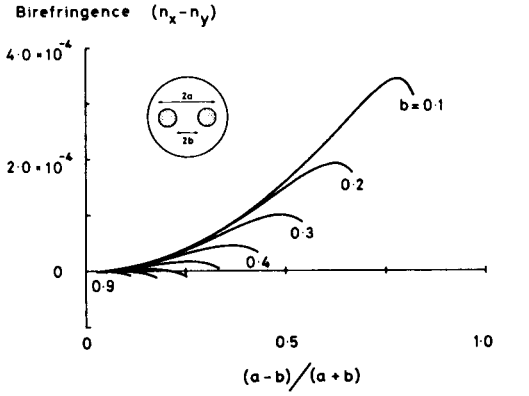

Fig. 6. Variation of modal birefringence with cross-sectional geometry in a fiber with circular stress-producing regions plotted for various values of b, the inner radius of the stress-producing regions.

assumption that the optical field is concentrated at $r = 0$ to calculate the birefringence is clearly invalid, since the stress varies rapidly with radius.

C. Fibers with Elliptical Stress-Producing Regions

Integrating (19) using Simpson's rule gives the birefringence curves plotted in Fig. 5, which are applicable to fibers in which the stress is produced either by using a high expansion core, or by an external elliptical stress-producing region in the cladding. We see that the magnitude of the birefringence is somewhat lower than that produced for the bow-tie structure (Fig. 4) for the same value of $(\Delta\alpha)\,T$, owing to the lower stress-utilization efficiency.

Note that there is now an advantage in having $a > r_0$ for $b < 0.2$, in apparent contradiction of our earlier statement that no asymmetrically disposed material should be contained outside a radius $r_0 = 0.76$ (unless the sense is changed as in Fig. 2(b)). In this case, the explanation is that the negative birefringence contribution of the material in $r > r_0$ is offset by the increased positive contribution of that in $r < r_0$ when a is increased. If we relax the artificial restriction that the stress-producing region should be elliptical and truncate the ellipse at r_0, we would obtain a higher birefringence for $b < 0.2$ than indicated by the curves.

The straight line obtained as $b \to 0$, corresponds to the case for infinite fiber outer dimension and is given by the contribution of the particular integral alone to (19). The equation of this line can be obtained from (19) by neglecting the complementary function term $(-3r^3)$, substituting for r from (20) and integrating using the substitution $x = \cos 2\phi$. The result agrees with Chu's analysis of an elliptical-core fiber with an infinite cladding, and is given by [8]

$$B = \frac{CE}{1-\nu}(\Delta\alpha)\,T\frac{(a-b)}{(a+b)}. \tag{24}$$

As shown by Chu [8], this equation shows excellent agreement with Okamoto *et al.*'s finite-element analysis of elliptical-core fibers [10]. The curves of Fig. 5 also show reasonable agreement with the finite element analysis of the elliptical-jacket fiber [12], [13] given by Namahira *et al.*

D. Fibers with Circular Stress-Producing Regions

Integrating equation (19) using Simpson's rule gives the birefringence curves shown in Fig. 6. For this structure (Fig. 2(e)), small values of B are obtained for small values of $(a-b)/(a+b)$ because of the sin 2ϕ term in (19), while large values of B are obtained for large values of $(a-b)/(a+b)$, since the structure approaches that of the bow-tie fiber. Thus from a birefringence point of view this structure presents no advantage.

E. Discussion

Although the structures shown in Fig. 2 look very different, the curves in Figs. 4–6 are remarkably similar. This should be expected from (17), since the structures all have a similar second-harmonic component. However, in terms of stress efficiency the bow-tie fiber is best, since the structure minimizes the *overall* stress levels for a given birefringence.

From Figs. 4–6 we are now in a position to suggest relative dimensions for the optimum internal asymmetries. For a fiber of normalized radius $r = 1$, the asymmetry should have an inner radius b as small as possible, consistent with the practical requirement that the optical power is confined to low-loss regions of deposited glass. This requirement normally restricts b to about 0.1–0.2, although the use of a large core index difference would confine the optical power nearer to the fiber axis and would allow the relatively lossy stress-producing regions to approach more closely. The outer radius a of the stress-producing zones should not exceed 0.76 of the fiber radius, unless restricted to a certain shape (e.g., elliptical), when some small advantage may be gained by relaxing this rule.

For each structure, the effect on the birefringence of reducing the substrate size can be seen by moving vertically downwards through the curves of Figs. (4) to (6). The effect can be drastic, more than halving the birefringence in some cases. This is an important observation, since the fiber diameter relative to the internal structure is often under the control of the fabricator, for example by sleeving the preform. A suitable choice of sleeve diameter could, therefore, considerably increase the resulting birefringence, although there is a maximum diameter above which little increase is expected. The effect is emphasized in the following experiment in which the fiber diameter was

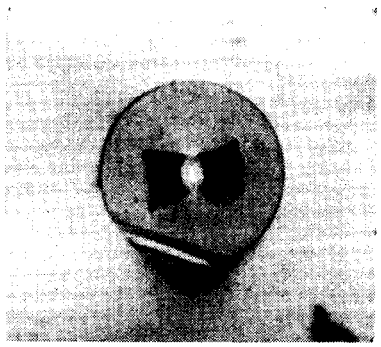

Fig. 7. Cross-section of the bow-tie fiber used in the experiment.

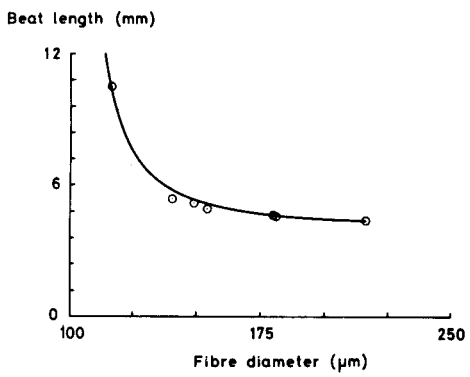

Fig. 8. Measured variation of polarization beat length in a bow-tie fiber as the fiber diameter was reduced by acid etching (points). The solid line is the predicted decrease in beat length.

successively reduced by etching and the birefringence was measured.

V. Experiment

The cross section of an early bow-tie fiber is shown in Fig. 7. The fiber was immersed in a 40-percent solution of hydrofluoric acid and the polarization beat length $L_p = \lambda/B$ was measured at a wavelength $\lambda = 633$ nm by observation of the transversely scattered light as the fiber diameter decreased. The results are shown in Fig. 8, together with the theoretical prediction obtained from (19). For the latter the fiber cross-sectional geometry was modeled using an ellipse of major and minor axes 21 and 14 μm, respectively, for the inner boundary of the sectors, followed by straight lines $y = \pm(0.16 \times +21)$ μm out to a radius of 52 μm. This procedure demonstrates the ease with which (19) can handle virtually any mirror-symmetric geometry. The fiber radius was 108 μm and $(\Delta\alpha)T$ was chosen as 2.9×10^{-3}, since this gave the best fit to the experimental data. Values of E, C, and ν were taken as before. The core of the fiber was elliptical and, therefore, exhibited some shape and stress birefringence of its own, estimated to be -7×10^{-5}. Although small, this was taken into account.

Reference to Fig. 8 shows that the agreement between theory and experiment is close and the important role of the substrate, therefore, verified. The experiment has been performed on a number of fibers with similar results, and can be used as a means of determining whether a particular fiber has sufficient substrate. From Fig. 8, we see that provided this fiber had a diameter greater than ~150 μm the birefringence is maximized; increasing the fiber diameter further has little effect on the birefringence.

VI. Conclusions

A simple and intuitive formula for stress-induced modal birefringence has been derived which is able to deal with virtually any cross-sectional geometry. This formula shows the following.

1) Only the second-harmonic component of the asymmetry contributes to the birefringence.

2) Other harmonics merely contribute to the general level of stress in the fiber and are undesirable. They produce extra stresses which may fracture the preform.

3) Circular regions of uniform expansion coefficient can be ignored in analyzing new structures.

4) In a fiber of normalized radius $r = 1$, asymmetries in $r > 0.76$ have an opposite contribution to asymmetries in $r < 0.76$ and, therefore, subtract from the birefringence.

The theory allows prediction of the optimum structure which maximizes the birefringence for a given expansion coefficient mismatch. If the dopant is confined in $r < 0.75$ then the optimum structure is the bow-tie fiber shown in Fig. 2(a) and realized in Fig. 7. Some additional birefringence can be obtained by siting dopant outside a radius of $r = 0.76$, provided it is located in quadrature, as shown in Fig. 2(b), or has an expansion coefficient less than that of silica.

Bow-tie, eliptical core, elliptical jacket, and circular side-pit fibers have each been analyzed. The results extend previous analyses by showing how a finite substrate reduces and can even reverse the sign of birefringence.

An etching experiment where the substrate of a bow-tie fiber was removed by acid etching has verified the considerable role of the substrate on the birefringence.

Acknowledgment

The authors would like to thank Dr. M. J. Adams of the Optical Communications Group and Dr. M. Petyt of the Institute of Sound and Vibration Research Unit of Southampton University for useful theoretical discussions.

References

[1] F. Fevre, L. Jeunhomme, I. Joindot, M. Monerie, and J.C. Simon, "Progress towards heterodyne-type single-mode fiber communication systems," *IEEE J. Quantum Electron.*, vol. QE-17, pp. 897-906, 1981.

[2] R. Ulrich and M. Johnson, "Fiber-ring interferometer: Polarisation analysis," *Opt. Lett.*, vol. 4, pp. 152-154, 1979.

[3] J. Sakai and T. Kimura, "Polarization behavior in multiply perturbed single-mode fibers," *IEEE J. Quantum Electron.*, vol. QE-18, pp. 59-65, 1982.

[4] V. Ramaswamy, W. G. French, and R. D. Standley, "Polarisation characteristics of noncircular core single-mode fibers," *Appl. Opt.*, vol. 17, pp. 3014-3017, 1978.

[5] J. D. Love, R. A. Sammut, and A. W. Snyder, "Birefringence in elliptically deformed optical fibres," *Electron. Lett.*, vol. 15, pp. 615-616, Sept. 27, 1979.

[6] T. Katsuyama, H. Matsumura, and T. Suganuma, "Low-loss single-polarisation fibres," *Electron. Lett.*, vol. 17, pp. 473-474, 1981.

[7] I. P. Kaminow and V. Ramaswamy, "Single-polarisation optical fibres: Slab model," *Appl. Phys. Lett.*, vol. 34, pp. 268-270, 1979.

[8] P. L. Chu, "Thermal stress induced birefringence in single-mode elliptical optical fibre," *Electron. Lett.*, vol. 18, pp. 45-47, 1982.
[9] J. Sakai and T. Kimura, "Birefringence caused by thermal stress in elliptically deformed core optical fibers," *IEEE J. Quantum Electron.*, vol. QE-18, pp. 1899-1909, 1982.
[10] K. Okamoto, T. Hosaka, and T. Edahiro, "Stress analysis of optical fiber by a finite element method," *IEEE J. Quantum Electron.*, vol. QE-17, no. 12, pp. 2123-2129, 1981.
[11] K. Okamoto, T. Hosaka, and Y. Sasaki, "Linearly single polarization fibers with zero polarization mode dispersion," *IEEE J. Quantum Electron.*, vol. QE-18, no. 4, pp. 496-503, 1982.
[12] Y. Namahira, Y. Ejiri, K. Mochizuki, "Birefringence in elliptically cladding single-polarisation fibres," *Electron. Lett.*, vol. 18, pp. 89-91, 1982.
[13] Y. Ejiri, Y. Namihira, and K. Mochizuki, "Stress difference in elliptically clad fibres," *Electron. Lett.*, vol. 18, pp. 603-605, 1982.
[14] P. L. Chu, "Finite element analysis of birefringence in azimuthally inhomogeneous optical fibre," *Electron. Lett.*, vol. 18, pp. 441-442, 1982.
[15] A. J. Barlow, D. N. Payne, M. P. Varnham, and R. D. Birch, "Polarisation characteristics of fibres for coherent detection systems," in *IEE Colloquium on Coherence in Optical Fibre Systems*, Dig. no. 1982/59.
[16] R. D. Birch, D. N. Payne, and M. P. Varnham, "Fabrication of polarisation-maintaining fibres using gas-phase etching," *Electron. Lett.*, vol. 18, pp. 1036-1038, 1982.
[17] S. Timoshenko and J. N. Goodier, *Theory of Elasticity*, 3rd ed. New York: McGraw-Hill, 1970.
[18] Y. Sasaki, K. Okamoto, T. Hosaka, and N. Shibata, "Polarisation-maintaining and absorption reducing fibres," in *Tech. Dig. Topical Meeting Opt. Fiber Commun.* (Phoenix, AZ), 1982.
[19] R. H. Stolen, R. E. Howard, and W. Pleibel, "Substrate-tube lithography for optical fibres," *Electron Lett.*, vol. 18, pp. 764-765, 1982.

*

Malcolm P. Varnham was born in Fareham, England on February 18, 1959. He joined British Aerospace in 1977 and was released to do a B.Sc. in electronics at the University of Southampton, Hampshire, England. In 1982, he joined the Optical Communications Group at the University of Southampton, where he is working for a Ph.D. degree on high birefringence in optical fibers.

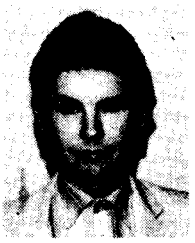

David N. Payne was born in Lewes, England, on August 13, 1944 and educated in Central Africa. He received the B.Sc. degree in electrical engineering, the Diploma in quantum electronics, and the Ph.D. degree from the University of Southampton, Southampton, England.

In 1972, he became the Pirelli Research Fellow in the Department of Electronics, University of Southampton and, in 1977, he was appointed to the Optical Communications Group as a Senior Research Fellow. Since 1969 his research interests have been in optical communications and have included preform and fiber fabrication techniques, optical propagation in multimode and single-mode fibers, fiber and preform characterization, wavelength-dispersive properties of optical-fiber materials optical transmission measurements, and fiber devices. Currently, his main fields of interest are polarization properties of optical fibers, fiber sensors, and optical transmission.

*

Arthur J. Barlow was born in Banbury, England on June 11, 1957. He received the B.Sc. degree in applied physics and electronics from the University of Durham, Durham, England in 1978. In 1978 he joined the Optical Communications Group, University of Southampton, Southampton, England as a Research Student working for the Ph.D. degree on birefringence properties of single-mode fibers.

In 1982 he joined British Aerospace and is presently on leave at Southampton University to continue his studies.

*

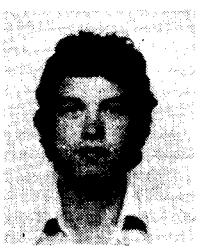

Robin D. Birch was born in Epsom, England in 1955. He graduated from the University of Kent at Canterbury, England, in 1977 and received a Ph.D. in 1981.

In 1980 he joined the Optical Communications Group at the University of Southampton as a Research Fellow. His current interests are in single-polarization fiber fabrication.